IEEE Access
Multidisciplinary | Rapid Review | Open Access Journal

Received July 10, 2019, accepted July 17, 2019, date of publication July 24, 2019, date of current version August 9, 2019.

Digital Object Identifier 10.1109/ACCESS.2019.2930773

Design Dual-Polarization Frequency Selective Rasorber Using Split Ring Resonators

XIMENG ZHANG, WEIWEI WU, YUHONG MA, CHANG WANG, CHENXIN LI, AND NAICHANG YUAN

State Key Laboratory of Complex Electromagnetic Environmental Effects on Electronics and Information System, National University of Defense Technology, Changsha 410073, China

Corresponding author: Weiwei Wu (wuweiwei_nudt@qq.com)

ABSTRACT A novel dual-polarization frequency selective rasorber with one transmission band and two absorbing bands is proposed in this paper. The structure is composed of a lossless frequency selective surface layer and a resistive layer. The resistive layer is a combination of split ring resonators and Jerusalem crosses. The frequency selective surface layer is a combination of grids and square rings. Split ring resonators are used to generate parallel resonances in this paper. When the parallel resonant frequency of the split ring resonators and that of the frequency selective surface layer are the same, a passband is obtained. Split ring resonators, Jerusalem crosses, and lumped resistors are used to create the absorbing bands. When surface current flows through two different paths on the split ring resonator, absorbing bands are obtained on each side of the passband. A frequency selective rasorber prototype is fabricated and measured to validate our design. The results show that the center frequency of the passband is 5.74 GHz, with an insertion loss of 0.25 dB. The lower and higher absorption bandwidths with absorption coefficient higher than 80% range from 1.92 to 3.73 GHz and from 7.41 to 9.34 GHz, respectively, and the reflection band with reflection coefficient less than −10 dB ranges from 1.96 to 9.32 GHz.

INDEX TERMS Frequency selective surfaces, frequency selection rasorber, radar cross section, absorption, transmission.

I. INTRODUCTION

Frequency selective surfaces (FSSs) are metallic arrays that are periodically arranged in a two-dimensional direction and act as bandstop or bandpass filters in three-dimensional space [1], [2]. Different FSS structures exhibit different transmission and reflection responses, which are essential for a wide range of applications in antennas, radomes and electromagnetic (EM) shields [3]–[5]. Radomes enclose antennas to protect them from external environments [6]. FSSs can be loaded on the radomes to ensure low transmission loss in the operating band while reflecting signals outside the bands for reducing the out-of-band monostatic radar cross section (RCS) of the antenna. However, with the developments of bistatic radars and multi-static radars, FSS radomes have been unable to meet the stealth requirements of the antennas. Absorbers have been widely used in various applications. They can reduce the reflection EM waves by absorption [7]–[9]. However, EM waves cannot pass through the absorber, so it is difficult to apply the absorber to the radome.

To reduce the strong RCS outside the operating band of the FSS radome, researchers have proposed a structure called frequency selective rasorber (FSR) that can be loaded onto a radome and has the properties of a FSS and an absorber at the same time. FSRs allow signals to pass through an antenna's operating band. They also absorb signals within a certain range outside the passband to protect the antenna system from out-of-band signals and reduce the RCS of the radome. In recent years, there has been an increasing amount of literatures on FSRs. In general, FSRs can be divided into 2-D and 3-D types. A 2-D FSR consists of one resistive layer and one lossless FSS layer separated by air. In [10], [11], low-frequency transmission and high-frequency absorption FSRs (T-A) are proposed. In [10], a FSR which consists of a square loop resistive film array and a metallic interdigitated Jerusalem cross array is proposed. The metallic array forms a passband at the lower band, and the resistive film absorbs EM waves in the reflection band. Magnetic materials have been used as resistive layers [11]. The structure can achieve

The associate editor coordinating the review of this manuscript and approving it for publication was Wen-Sheng Zhao.

angular-stable performance. However, the problem is that the absorbing band and the passband are far apart. In [12]–[15], high-frequency transmission and low-frequency absorption FSRs (A-T) are proposed. Parallel resonances can be introduced into the resistive layer to produce an infinite impedance which results in one transmission path. A tiny strip-type parallel LC structure is inserted in the center of a metallic dipole element. When the trip-type structure is parallel resonant, one passband is obtained [12], [13]. A dipole array loaded with lumped resistors is used as a resistive layer. Only one lumped resistor is loaded in each unit cell to reduce fabrication cost [14]. In [15], the lumped resistors and circular spiral resonators are loaded on a hexagonal metal ring. Compared with other structures, this structure shows a smaller size and a wider passband. Since the above two types of FSRs can only achieve one-side absorbing (T-A and A-T), FSRs having one absorbing band on each side of the transmission band (A-T-A) have been proposed in [16]–[20]. The resistive film has also been used in resistive layer to achieve A-T-A [16], [17]. Although such a design is simple, there still exist surface current on the resistive film in the passband, resulting in high insertion loss. In [18], the square-loop hybrid resonator is used in the resistive layer to generate parallel resonance. The results show that the FSR has a wide operating bandwidth ($|S_{11}| < -10$dB), but it is sensitive to both TE and TM polarizations. As the incident angle increases, the insertion loss increases rapidly. In [19], the inductor and the capacitor are simplified to a microstrip structure, and the parameters of the equivalent circuit model can be calculated from the actual physical size. However, the absorption coefficient near the transmission band is not sufficient, which is disadvantageous for the reduction of the RCS. In [20], eight resistors are loaded on one miniaturized cross-frame unit. The FSR has wide operating and passband bandwidths, but too many resistors lead to higher costs and fabricating difficulties. Compared to 2-D FSRs, 3-D FSRs show wider bandwidths, higher selectivity and better stability under oblique incidences. Unfortunately, they are large in size and not easy to fabricate [21]–[24].

In this paper, a dual-polarized FSR with a passband and two absorbing bands, which is realized through combination of split ring resonators and Jerusalem crosses is proposed. The equivalent circuit model (ECM) and surface current distribution are given to illustrate the principle of absorbing and transmitting. The performance of the FSR under oblique incidence is investigated. Moreover, the bistatic RCS reduction of FSR under normal incidence is also studied. To validate our design, a prototype is fabricated and measured.

II. DESIGN AND ANALYSIS OF THE FSR

A two-layer FSR which consists of a resistive layer and an FSS layer is proposed in Fig. 1 (g). Fig. 1 (a) - (e) show the evolution of the resistive layer. Fig. 1 (a) and (b) display the dipole with end loadings and SRR, respectively. Fig. 1 (c) is the combination of (a) and (b), in which the SRR is placed in the center of the dipole unit and two resistors are loaded

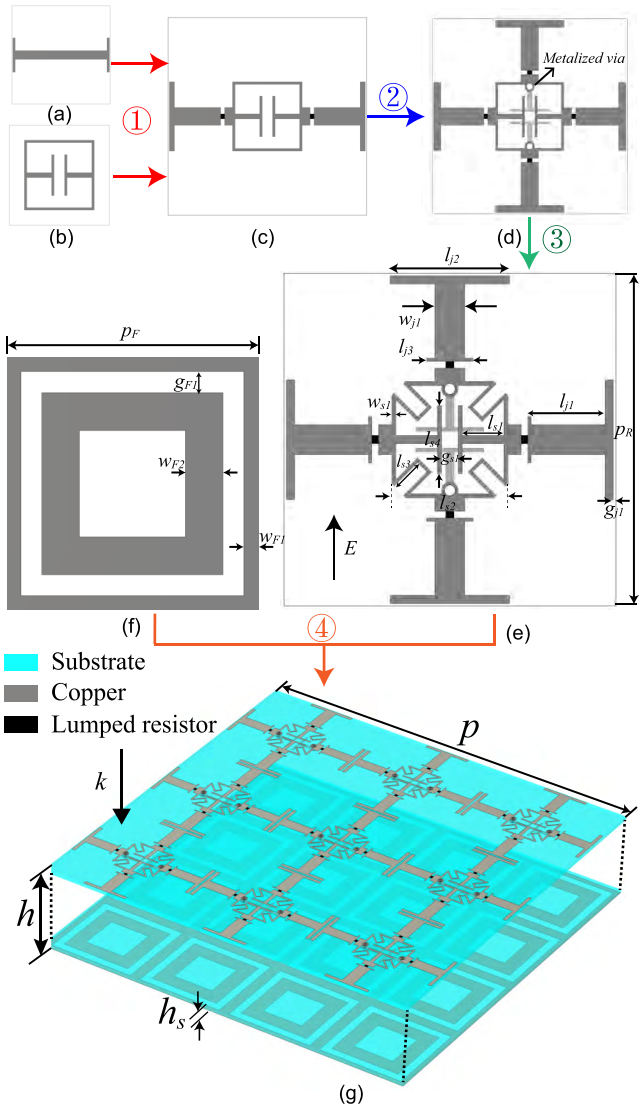

FIGURE 1. (a) dipole with end loading, (b) SRR, (c) the simple single polarized resistive layer, (d) the simple dual polarized resistive layer, (e) one unit of the resistive layer with folded arms, (f) one unit of FSS, (g) one unit of FSR. (F = FSS, j = jc and s = SRR) (Physical dimensions: $p_F = 15$, $g_{F1} = 1.25$, $w_{F2} = 0.825$, $w_{F2} = 2.25$, $p_R = 20$, $l_{j1} = 4.65$, $l_{j2} = 7$, $l_{j3} = 2.8$, $g_{j1} = 0.15$, $w_{j1} = 1.8$, $l_{s1} = 2.5$, $l_{s2} = 7$, $l_{s3} = 2$, $l_{s}4 = 4.1$, $g_{s1} = 1$, $w_{s1} = 0.25$, $p = 60$, $h = 13$, $h_s = 0.5$. Unit: mm, $R = 130\ \Omega$).

on the dipole near the SRR. Fig. 1 (d) is the dual-polarization model which is modified from (c). A dual-polarized SRR is loaded at the center of the Jerusalem cross. Since the inner arms of the dual-polarized SRR overlap each other, the inner arms in the other direction are loaded on the back layer of the substrate and are connected to the upper layer through the metallized vias. In (e), the four corners of the ring of the SRR are folded. Vertical arms are printed near the resistors but away from the SRR. The size of the resistive layer unit is different from that of the FSS unit. The ratio of the number of cells in the resistive layer to the FSS layer is 9:16, and the period of the FSR $p = 60$ mm. The resistive layer and the FSS layer are supported by F4BM, which has a relative

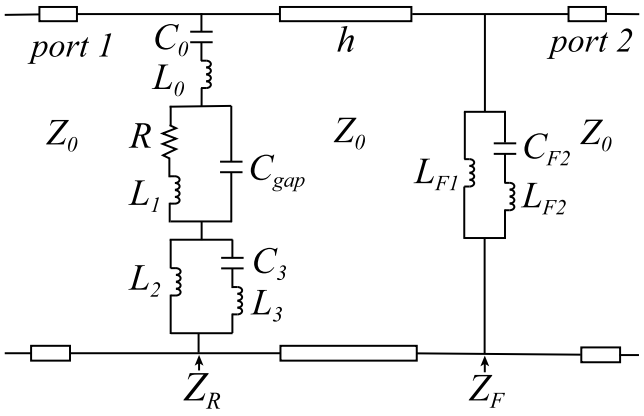

FIGURE 2. The ECM of the FSR. (Circuit parameters: $C_0 = 0.2$ pF, $L_0 = 7.28$ nH, $R = 280\ \Omega$, $L_1 = 2.38$ nH, $C_{gap} = 0.047$ pF, $L_2 = 0.75$ nH, $C_3 = 0.23$ pF, $L_3 = 2.72$ nH, $L_{F1} = 4.6$ nH, $C_{F2} = 0.13$ pF, $L_{F2} = 1.55$ nH, $h = 13$ mm, $Z_0 = 377\ \Omega$).

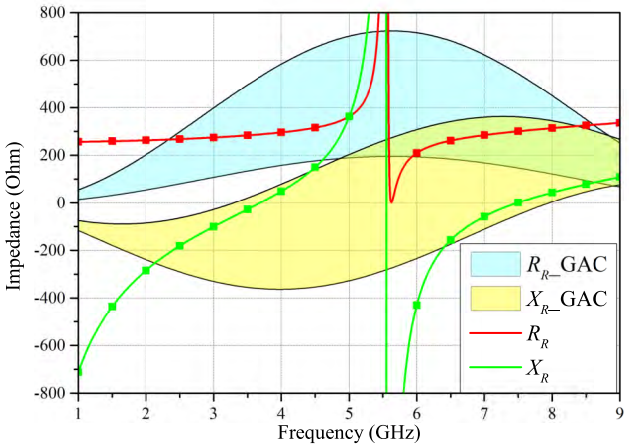

FIGURE 3. Equivalent impedance of resistive sheet and GAC for a 13-mm-thick absorber.

permittivity of 2.55, a loss tangent of 0.0007, and a thickness of 0.5 mm.

Fig. 2 shows the ECM of the proposed FSR. Z_R and Z_F are the impedances of the resistive layer and the FSS layer, respectively. For the sake of analysis simplicity, we assume that the impedance of the spacer between the resistive layer and the FSS layer is equal to the free space wave impedance Z_0 and the thickness of the spacer is h which is usually one quarter of the passband wavelength f_0. In the ECM, C_0 represents the capacitance of Jerusalem crosses in adjacent cells. L_0 and L_1 represent the outer and inner arms of the Jerusalem cross divided by the resistor R, respectively. There are two capacitances, one is between the inner and outer arms of the Jerusalem cross, the other is between the inner arm of the Jerusalem cross and the ring of the SRR. For the sake of simplicity, we use C_{gap} to represent their capacitances. L_2 and L_3 represent the inductance of the ring and the inner arms of the SRR, respectively. C_3 represents the capacitance between the end loadings on the inner arms of the SRR. The FSS is composed of the gridded-square arrays [26]. L_{F1} and L_{F2} represent the inductance of the grid and the square ring, respectively. C_{F2} represents the capacitance between the grid and the square ring.

For the A-T-A type FSR, we assume that its passband is obtained at f_0 and the lower and higher absorbing bands are obtained at f_1 and f_2, respectively. In the passband,

$$|S_{21}| = 1, |S_{11}| = 0 \tag{1}$$

while in the absorbing band,

$$|S_{21}| = 0, |S_{11}| = 0 \tag{2}$$

The absorbing rate can be equivalent to the following:

$$A = 1 - |S_{21}|^2 - |S_{11}|^2 \tag{3}$$

When the FSS is illuminated by EM waves, the FSS reflects or transmits the EM waves. We choose the band-pass FSS to generate the passband. In the reflection band of the FSS, the incident EM wave is reflected, which can be equivalent to a ground plane, so the FSR is equivalent to an absorber in the reflection band of the FSS. Therefore, the combined structure of the two can achieve transmission and absorption in different frequency bands.

When L_{F1} and $C_{F2}\&L_{F2}$ are in parallel resonance, the current does not pass through the FSS layer. Consequently, a passband is obtained at the resonance point, and its frequency f_{Fp} can be written as follows:

$$f_{Fp} = \frac{1}{2\pi\sqrt{(L_{F1} + L_{F2})\, C_{F2}}} \tag{4}$$

When current flows through the resistive layer, energy will be consumed by the resistor R. So, the resistive layer should be open-circuited in the passband, which can be achieved by parallel resonance of L_2 and $C_3\&L_3$. The resonant frequency f_{Rp} can be written as follows:

$$f_{Lp} = \frac{1}{2\pi\sqrt{(L_2 + L_3)\, C_2}} \tag{5}$$

Only when the current passes through neither the resistive layer nor the FSS layer, one passband can be obtained. So $f_0 = f_{FP} = f_{RP}$. From Fig. 2, we know that the center frequency of the passband is 5. 63GHz.

In the ECM, Z_R can be expressed as follows:

$$Z_R = \frac{A}{jwC_0} + \frac{R + jwL_1}{1 + wC_{cap}(jR - wL_1)} + \frac{jwL_2B}{B - w^2L_2C_3} \tag{6}$$

And Z_F can be expressed as follows:

$$Z_F = \frac{jwL_{F1}D}{D - w^2L_{F1}C_{F2}} \tag{7}$$

in which $\omega = 2\pi f$, $A = 1 - w^2L_0C_0$, $B = 1 - w^2L_3C_3$ and $D = 1 - w^2L_{F2}C_{F2}$.

The FSS passes EM waves in the passband and it reflects EM waves outside the passband. When we investigate the absorbing properties of the FSR, we replace the FSS with a metal plate making the FSR become an absorber. The center frequency of the absorptive band is approximately one quarter of the absorber. Fig. 3 shows the general absorption condition (GAC) of a 13-mm-thick absorber and the equivalent

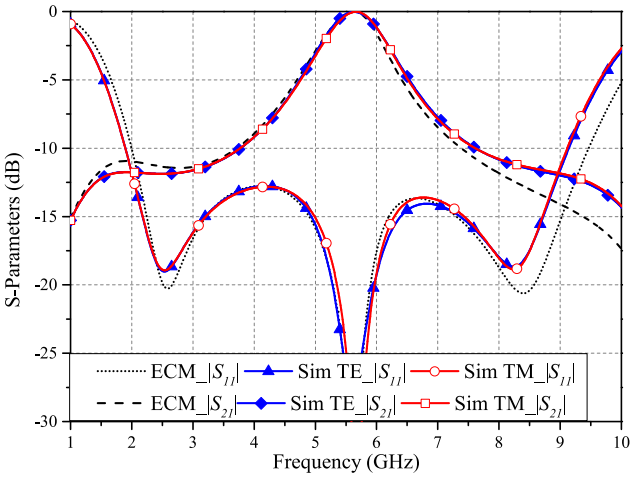

FIGURE 4. The S parameter of the ECM results and simulation results under normal incidence.

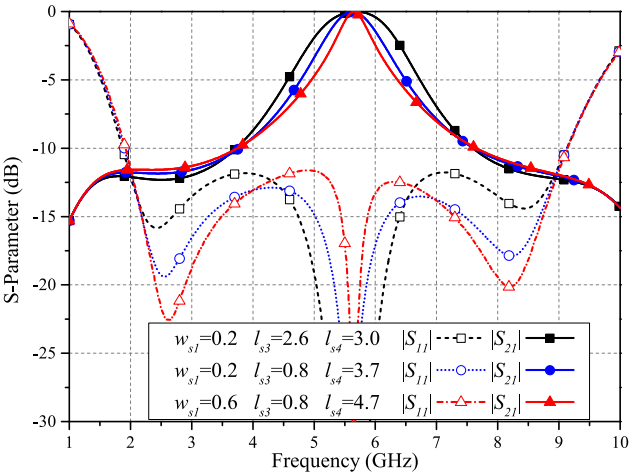

FIGURE 5. The S parameter of the FSR with different w_{s1}, l_{s3}, and l_{s4} under normal incidence.

impedance of the resistive layer. When the impedance of the resistive layer meets GAC, good absorbing properties ($|S_{11}| \leq -10$dB) are obtained [27].

Z_R is the equivalent impedance of the resistive layer calculated by (6). R_R and X_R are the real and imaginary parts of Z_R, respectively ($Z_R = R_R + jX_R$). We can see that Z_R meets GAC when R_R meets R_R_GAC and X_R meets X_R_GAC in the ranges of 2.36 - 4.42 GHz and 6.38 - 8.65 GHz. It means that the $|S_{11}|$ of the absorber is reduced by at least 10 dB in the two bands. It is worth noting that at 5.63 GHz, the impedance of the resistive layer becomes very high, which means that EM waves are hardly absorbed at this frequency point.

The ABCD matrix of the double-layered FSR can be written as follows:

$$\begin{bmatrix} A & B \\ C & D \end{bmatrix} = \begin{bmatrix} 1 & 0 \\ \frac{1}{Z_R} & 1 \end{bmatrix} \begin{bmatrix} \cos\beta h & jZ_0 \sin\beta h \\ j\frac{\sin\beta h}{Z_0} & \cos\beta h \end{bmatrix} \begin{bmatrix} 1 & 0 \\ \frac{1}{Z_F} & 1 \end{bmatrix} \tag{8}$$

where $\beta = 2\pi f_0/c$, and c is the speed of light in vacuum.

The reflection coefficient and the transmission coefficient can be written by the ABCD matrix as follows:

$$|S_{11}| = \left| \frac{-\frac{Z_0 P}{\tan\beta h} + jZ_0(Z_R - Z_F - Z_0)}{\frac{2Q+Z_0 P}{\tan\beta h} + j({Z_0}^2 + Z_0 P + 2Q)} \right| \tag{9}$$

$$|S_{21}| = \left| \frac{2}{\left(\frac{Z_0 P}{Q} + 2\right)\cos\beta h + j\left(\frac{Z_0(Z_0+P)}{Q} + 2\right)\sin\beta h} \right| \tag{10}$$

in which, $P = Z_R + Z_F$, and $Q = Z_R Z_F$.

The FSR we designed is simulated in CST Microwave Studio. Fig. 4 compares the ECM results obtained by (9) and (10) with our simulation results under normal incidence. It can be seen that the simulation results are similar to the ECM results. Some small differences may be attributed to the effect of the dielectric plates. The simulated TE polarization and TM polarization results are basically coincident. Therefore, in the following part, we only present the performance of the FSR under TM-polarized oblique incidence. However, at approximately 6.7 GHz, the reflection coefficients of the two polarizations differ by 0.5 dB because the influence of the parasitic effect of the via under TE-polarized incidence is not completely eliminated. The result shows that the passband is located at 5.63 GHz, and its insertion loss is only 0.03 dB. The 3 dB bandwidth of the passband ranges from 5.02 to 6.27 GHz. The operation band ($|S_{11}| < -10$dB) ranges from 1.9 to 9.16 GHz, corresponding to a relative bandwidth of 131.3%. The frequency range with absorbing coefficient greater than 80% can be calculated by (3), which is from 1.81 to 4.2 GHz and from 7.03 to 9.25 GHz. It means that EM waves are greatly absorbed outside the passband, and the reflected waves are effectively reduced.

Different passband bandwidths are required in different applications. The bandwidth can be simply changed by L_2 and C_3 of the parallel resonance. It can be seen from Fig 3(e) that reducing the width of the SRR ring or increasing the length of the folded arm will increase L_2. Increasing the length of the end loadings of the SRR will increase C_3. To keep the center frequency of the passband unchanged, L_2 and C_3 need to satisfy (5). As seen from Fig. 5, the bandwidth is varied by adjusting w_{s1}, l_{s3}, and l_{s4}. Increasing l_{s4} and w_{s1} while decreasing l_{s3}, will reduce the 3 dB passband bandwidth from 32.9% to 14.6%, and the reflected waves in f_1 and f_3 are greatly reduced. At the same time, the operational bandwidth of the reflection band has hardly changed. Thus, we can change the passband bandwidth of the FSR by simply adjusting the value of the SRR.

Compared to the model in Fig. 1 (d), the model in Fig. 1 (e) not only adds the folding arms of the SRR but also adds the vertical arms near the resistors. Fig. 6 shows the performance of the FSR with different arm lengths l_{j3}. When l_{j3} is increased, the reflection coefficient changes more obviously than the transmission coefficient, and the impedance matching of the lower absorbing band is slightly better. In contrast, the impedance matching within the higher absorbing band is worse. When $l_{j3} = 3.7$ mm, the highest reflection coefficient

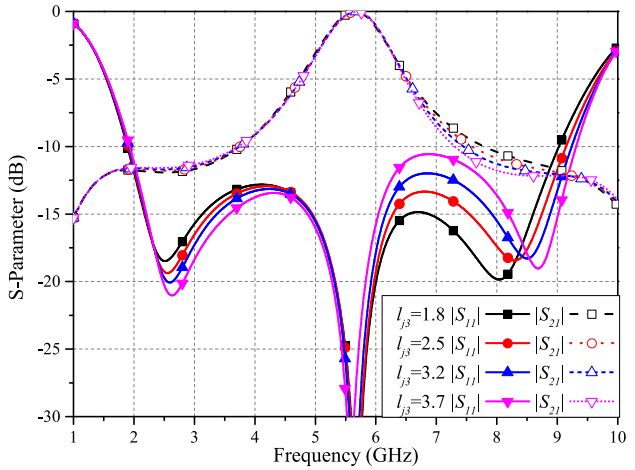

FIGURE 6. The S parameter of the FSR with different l_{j3} under normal incidence.

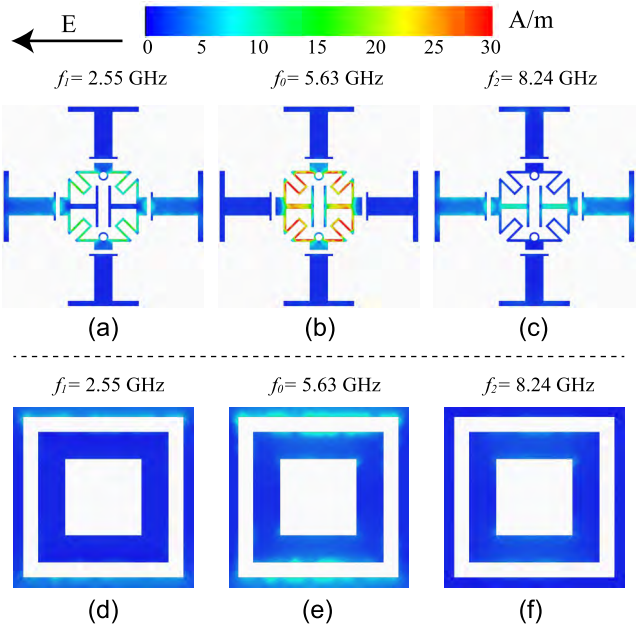

FIGURE 7. Surface current distribution of the resistive layer and FSS layer at $f_1 = 2.55$ GHz, $f_0 = 5.63$ GHz, and $f_2 = 8.24$ GHz, respectively.

in the higher absorption band is almost −10 dB. However, the high frequency absorbing point f_2 moves to the higher frequency, resulting in a wider operating bandwidth.

To better understand the mechanisms of transmission, reflection and absorption, the surface current distributions of FSR at f_0, f_1 and f_2 are investigated. It can be seen from Fig. 7 (b) that there is a strong current flow in the outer and inner arms of the SRR at f_0, resulting from the parallel resonance of the SRR. Similarly, in Fig. 7 (e), the current flowing on the grid and square rings of the FSS is due to the parallel resonance of the FSS layer. Since both FSS and SRR parallel resonances occur at f_0, a passband is obtained. It is worth noting that in Fig. 7 (b), the current is trapped in the SRR. There is almost no current flowing near the lumped resistors, meaning that the passband has only a very low insertion loss. Fig. 7 (a) and (c) are the surface current distributions of the resistive layer at the two absorbing points f_1 and f_2, respectively. In both Fig. 7 (a) and (c), current flows through the resistors, indicating that energy is being consumed and the absorbing bands are obtained. The difference is the current paths in the SRR. In Fig. 7 (a), current flows through the outer ring, while in Fig. 7 (b), current flows through the inner arms. This is because the outer and inner arm distributions of the SRR and the Jerusalem cross occur in series resonance, forming two different frequency absorption bands.

The size of the resistive layer unit and that of the FSS unit are both less than one-half of the passband wavelength of 26.6 mm. The small period is convenient for loading on the radomes with complex shapes, and it can attenuate the effect of the grating lobes. The performances of the FSR under oblique incidences are shown in Fig. 8. In Fig. 8 (a), the FSR is illuminated by the TE-polarized wave. As the incident angle increases, the transmission coefficient on both sides of the passband decreases. The reflection coefficient increases in the lower absorbing band, and the operating bandwidth is reduced at the high frequency. When the incident angle is within 30 degrees, the operating band is continuous. In Fig. 8 (b), we can see that the lower absorption band is insensitive to the incident angle, but the higher absorption bandwidth decreases with the angle, and the bandwidth with the absorption rate greater than 80% is reduced. In Fig. 8 (c), the FSR is illuminated by the TM-polarized wave. With the increase in the incident angle from 0 to 35 degrees, the transmission coefficient and the reflection coefficient on the left side of the passband both increase. On the right side, a transmission zero point moves from the high frequency to 9.43 GHz and the reflection coefficient exhibits a steep drop-off, which may be caused by the change in the electrical length. It can be seen from Fig. 8 (d) that the lower absorption bandwidth decreases slightly with the increasing angle. In contrast, the higher absorption bandwidth increases. In general, the proposed FSR is insensitive to the incident angle, which is contributed by the miniaturized unit of the resistive layer and the FSS layer.

Fig. 9 compares the bistatic RCS performances of the FSS and FSR at f_0, f_1 and f_2. Both the FSS and the FSR are with an array of 300 mm × 300 mm, and the incident angle of the EM wave is 0 degree. In Fig.9 (b), because energy is transmitted in the passband, both FSS's and FSR's bistatic RCSs are very low at f_0. Fig. 9 (a) indicates that the maximum RCS in the main lobe is reduced by 22 dB compared to the RCS of FSS at f_1. The maxima of the first side lobes are reduced by 16.9 dB and 17 dB compared to the RCS of FSS in the E and H planes, respectively. Fig. 9 (c) demonstrates that the maximum RCS in the main lobe is reduced by 17.1 dB compared to the RCS of FSS at f_2. Both in the E and H planes, the RCS reduction is higher than 10 dB within the first three side lobes. Fig. 9 demonstrates that our FSR has excellent absorbing performance and has better RCS reduction than FSS.

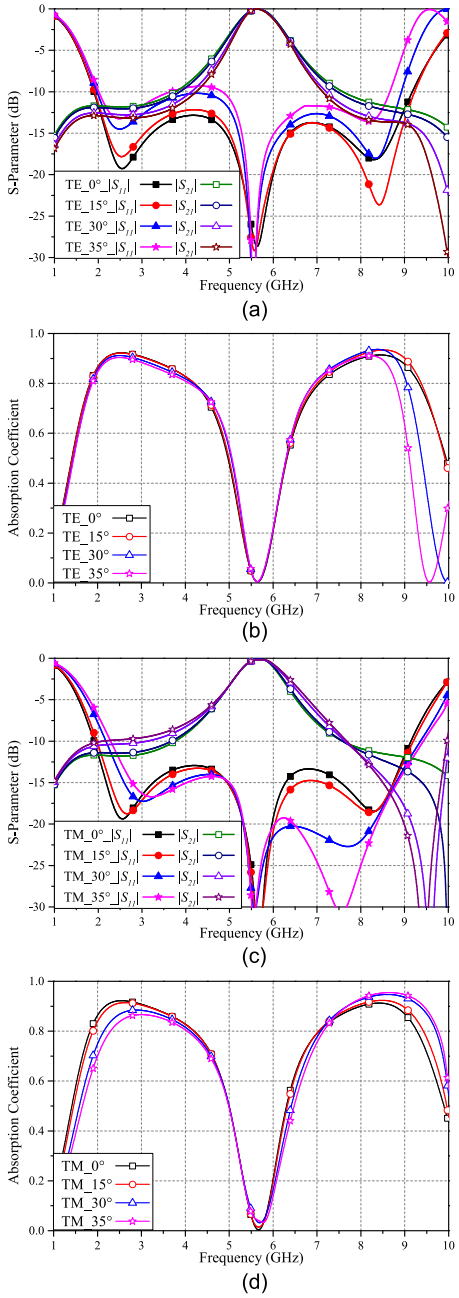

FIGURE 8. Simulated performances under oblique incidence. (a)(b) TE polarization. (c)(d) TM polarization.

III. EXPERIMENTAL RESULTS

To verify the design of our FSR, a FSR prototype is fabricated and measured as shown in Fig 10. The prototype contains a total of 15 × 15 resistive layer units and 20 × 20 FSS units, which means that the number of FSR units is 5 × 5. A total of 900 chip resistors with a resistance of 130 Ω are mounted on the resistor layer by surface mounting technology (SMT). The FSS layer and the resistive layer are isolated by bolts and nuts. Due to the large size of the FSR prototype, a foam plate with a relative permittivity of 1 is also used to support the PCB to reduce deformation. The measurement is carried out in an anechoic chamber. When measuring $|S_{21}|$, the FSR

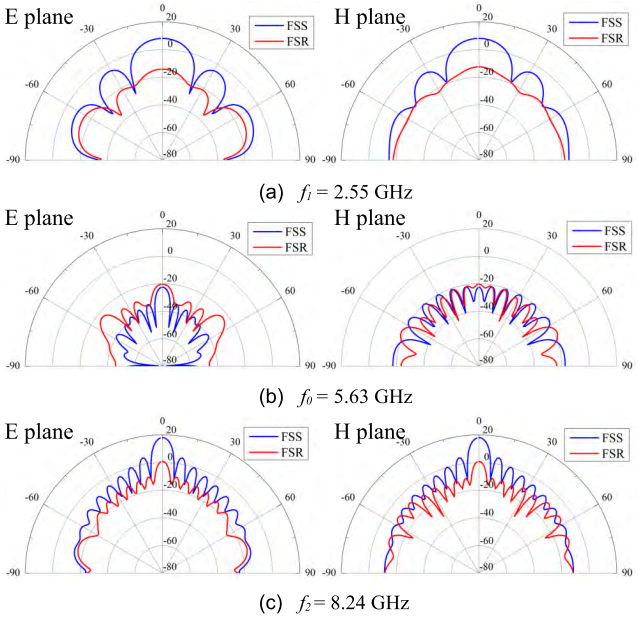

FIGURE 9. Comparison of FSS and FSR bistatic RCS performances under normal incidence at (a) $f_1 = 2.55$ GHz, (b) $f_0 = 5.63$ GHz, and (c) $f_2 = 8.24$ GHz, respectively.

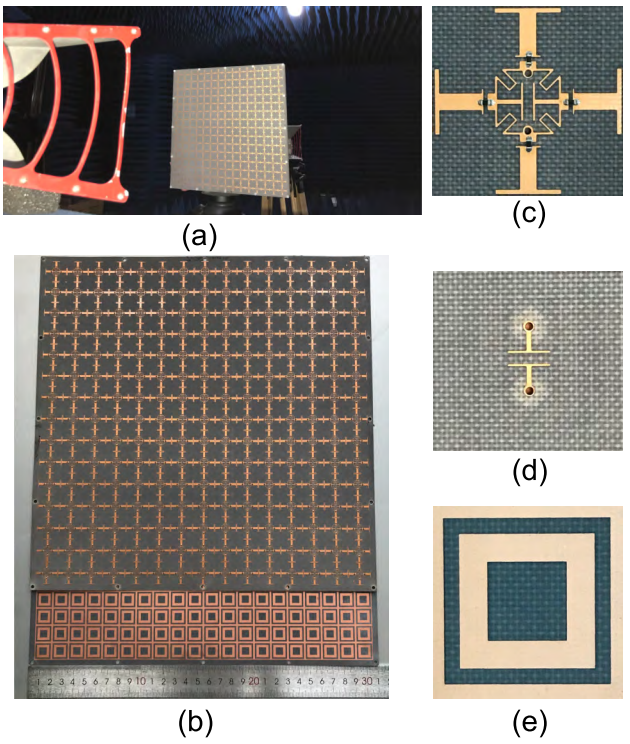

FIGURE 10. (a) Measurements in an anechoic chamber. (b) Photos of the fabricated FSR. (c) Front side of the resistive layer unit. (d) Back side of the resistive layer unit. (e) FSS layer unit.

prototype is placed between two standard gain horns. The resistive layer faces transmitting (Tx) antenna and the FSS layer faces receiving (Rx) antenna. $|S_{21}|$ is obtained by a vector network analyzer connected to the antennas. When measuring $|S_{11}|$, the resistive layer faces both the Tx and Rx antennas. First, a metal plate of the same size as that of

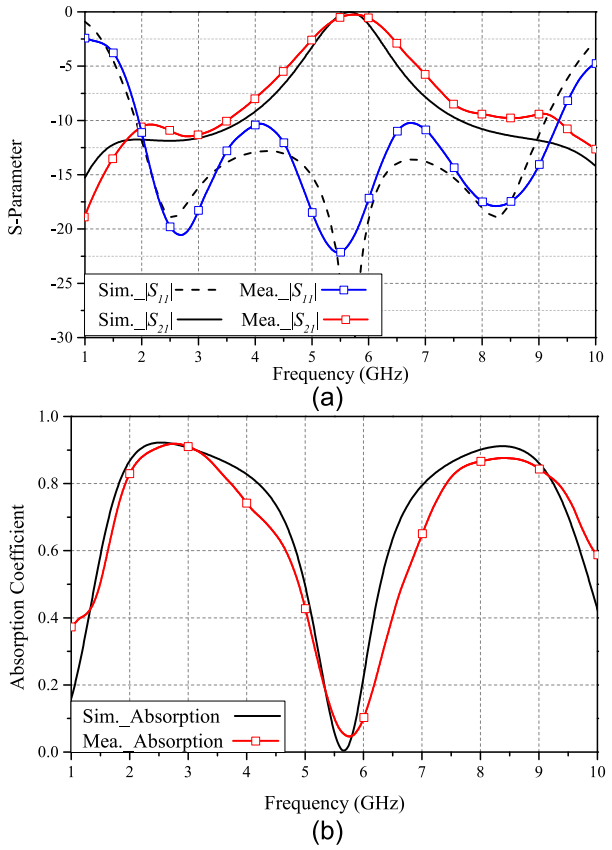

FIGURE 11. (a) Simulated and measured S-parameters under normal incidence. (b) Simulated and measured absorption coefficient.

the FSR is used to replace the FSR prototype for calibration. Then the metal plate is replaced with the prototype to measure $|S_{11}|$.

The comparisons of S parameter between the simulations and measurements are shown in Fig 11 (a). The center frequency of the measured passband shifts to the higher frequency of 5.74 GHz with an insertion loss of 0.25 dB. We attribute it to the manufacturing tolerances of the PCB. The operating bandwidth is from 1.96 to 9.32 GHz which means it has a relative bandwidth of 130.5%. The measured $|S_{11}|$ becomes higher with respect to the simulated value, Moreover, the $|S_{11}|$ between the absorbing bands and the passband are almost equal to -10 dB. This may be due to the coupling of the two antennas in the $|S_{11}|$ measurement and the multipath interference from the measurement environment. Additionally, the incident angle is too large to represent the normal incident wave. A comparison of the simulated and measured absorbing coefficients is shown in Fig 11 (b), The measured absorbing coefficients greater than 80% range from 1.92 to 3.73 GHz and from 7.41 to 9.34 GHz. It has a narrower bandwidth than the simulated one. The high-frequency absorption band moves to the higher frequency, and the absorption coefficient of the passband increases by 0.15. To illustrate the advantages of our FSR, the proposed FSR and the FSR from other literatures are compared in Table 1. It can be seen that our FSR has the advantages of a wider

TABLE 1. Performance comparison with previous FSR.

Ref.	FBW	LAB	HAB	IL (dB)	Thickness (λ_L)
[18]	129.1%	91.4%	31.9%	0.6	0.091
[20]	104.2%	N.A.	N.A.	0.73	0.098
[21]	108.4%	43.2%	15.3%	0.5	0.19
[23]	130%	25%	74.5%	0.73	0.187
[27]	112.4%	79.3%	29%	0.3	0.103
[28]	102.2%	59.9%	35.3%	0.63	0.15
[29]	98.3%	51.4%	40.8%	0.35	0.11
This (Sim.)	131.3%	79.5%	27.3%	0.03	0.082
Work (Mea.)	130.5%	64.1%	23%	0.25	0.085

FBW = fractional bandwidth of -10 dB reflection, LAB = lower absorption bandwidth for 80% absorption rate, HAB = higher absorption bandwidth for 80% absorption rate, IL = insertion loss, λ_L = free space wavelength at lowest frequency of - 10 dB reflection.

FBW, a lower insertion loss and a lower profile. Especially, the position and bandwidth of the transmission band can be easier to adjust by changing the dimensions of SRR.

IV. CONCLUSION

The paper introduces a new type of FSR. Through ECM and surface current distribution, we know that the passband of this FSR is determined by SRR and FSS. When in the passband, the current is trapped in the SRR, resulting in low insertion loss. The results show that the FSR has a wide operating band, performs well within 35 degrees of oblique incidence and exhibits excellent bistatic RCS reduction performance over FSSs. Finally, a prototype is fabricated and measured in an anechoic chamber to verify our design. Our proposed FSR can be applied to the radomes to improve the stealth performance of the platform.

REFERENCES

[1] B. A. Munk, *Frequency Selective Surfaces: Theory and Design*. New York, NY, USA: Wiley, 2000.
[2] R. Mittra, C. H. Chan, and T. Cwik, "Techniques for analyzing frequency selective surfaces-a review," *Proc. IEEE*, vol. 76, no. 12, pp. 1593–1615, Dec. 1988.
[3] W. Wu, X. Liu, K. Cui, Y. Ma, and Y. Yuan, "An ultrathin and polarization-insensitive frequency selective surface at Ka-band," *IEEE Antennas Wireless Propag. Lett.*, vol. 17, no. 1, pp. 74–77, Jan. 2018.
[4] H. Wang, L. Zheng, M. Yan, J. Wang, S. Qu, and R. Luo, "Design and analysis of miniaturized low profile and second-order multi-band polarization selective surface for multipath communication application," *IEEE Access*, vol. 7, pp. 13455–13467, 2019.
[5] W. Y. Yong, S. K. A. Rahim, M. Himdi, F. C. Seman, D. L. Suong, M. R. Ramli, and H. A. Elmobarak, "Flexible convoluted ring shaped FSS for X-band screening application," *IEEE Access*, vol. 6, pp. 11657–11665, 2018.
[6] D. J. Kozakoff, *Analysis of Radome-Enclosed Antennas*. Boston, MA, USA: Artech House, 2000.
[7] C. M. Watts, X. Liu, and W. J. Padilla, "Metamaterial electromagnetic wave absorbers," *Adv. Mater.*, vol. 24, no. 23, pp. OP98–OP120, 2012.
[8] F. Costa, A. Monorchio, and G. Manara, "Analysis and design of ultra thin electromagnetic absorbers comprising resistively loaded high impedance surfaces," *IEEE Trans. Antennas Propag.*, vol. 58, no. 5, pp. 1551–1558, May 2010.
[9] J. Yang and Z. Shen, "A thin and broadband absorber using double-square loops," *IEEE Antennas Wireless Propag. Lett.*, vol. 6, pp. 388–391, 2007.
[10] F. Costa and A. Monorchio, "A frequency selective radome with wideband absorbing properties," *IEEE Trans. Antennas Propag.*, vol. 60, no. 6, pp. 2740–2747, Jun. 2012.

[11] H. Zhou, L. Yang, S. Qu, K. Wang, J. Wang, H. Ma, and Z. Xu, "Experimental demonstration of an absorptive/transmissive FSS with magnetic material," *IEEE Antennas Wireless Propag. Lett.*, vol. 13, pp. 114–117, 2014.
[12] Q. Chen, L. Liu, L. Chen, J. Bai, and Y. Fu, "Absorptive frequency selective surface using parallel LC resonance," *Electron. Lett.*, vol. 52, no. 6, pp. 418–419, Mar. 2016.
[13] Q. Chen, S. Yang, J. Bai, and Y. Fu, "Design of absorptive/transmissive frequency-selective surface based on parallel resonance," *IEEE Trans. Antennas Propag.*, vol. 65, no. 9, pp. 4897–4902, Sep. 2017.
[14] Z. Wang, Q. Zeng, J. Fu, W. Chen, B. Lv, M. Song, and T. A. Denidni, "A high-transmittance frequency-selective rasorber based on dipole arrays," *IEEE Access*, vol. 6, pp. 31367–31374, 2018.
[15] Q. Chen, D. Sang, M. Guo, and Y. Fu, "Miniaturized frequency-selective rasorber with a wide transmission band using circular spiral resonator," *IEEE Trans. Antennas Propag.*, vol. 67, no. 2, pp. 1045–1052, Feb. 2019.
[16] W. Weiwei, C. Xi, F. Qi, Z. Xiaofa, and Z. Chang, "A measured FSS radome with two absorptive bands separated by one passband," in *Proc. 11th Eur. Conf. Antennas Propag. (EUCAP).*, Mar. 2017, pp. 1118–1121.
[17] W. Wu, M. Tianzhen, H. Jingjian, H. Yan, and D. Xiangyu, "Study of a metamaterial with single passband between two neighboring absorptive bands," in *Proc. 10th Eur. Conf. Antennas Propag.*, Apr. 2016, pp. 1–4.
[18] H. Huang and Z. Shen, "Absorptive frequency-selective transmission structure with square-loop hybrid resonator," *IEEE Antennas Wireless Propag. Lett.*, vol. 16, pp. 3212–3215, 2017.
[19] Z. Sun, Q. Chen, M. Guo, H. Yu, and Y. Fu, "Frequency selective rasorber and reflector with two-sided absorption bands," *IEEE Access*, vol. 7, pp. 6025–6031, 2019.
[20] X. Xiu, W. Che, Y. Han, and W. Yang, "Low-profile dual-polarization frequency-selective rasorbers based on simple-structure lossy cross-frame elements," *IEEE Antennas Wireless Propag. Lett.*, vol. 17, no. 6, pp. 1002–1005, Jun. 2018.
[21] Z. Shen, J. Wang, and B. Li, "3-D frequency selective rasorber: Concept, analysis, and design," *IEEE Trans. Microw. Theory Techn.*, vol. 64, no. 10, pp. 3087–3096, Oct. 2016.
[22] Y. Yu, G. Q. Luo, A. A. Omar, X. Liu, W. Yu, Z. C. Hao, and Z. Shen, "3D absorptive frequency-selective reflection and transmission structures with dual absorption bands," *IEEE Access*, vol. 6, pp. 72880–72888, 2018.
[23] Y. Yu, Z. Shen, T. Deng, and G. Luo, "3-D frequency-selective rasorber with wide upper absorption band," *IEEE Trans. Antennas Propag.*, vol. 65, no. 8, pp. 4363–4367, Aug. 2017.
[24] Y. Yu, G. Q. Luo, Q. Liu, W. Yu, H. Jin, Z. Liao, and Z. Shen, "3D band-absorptive frequency selective rasorber: Concept and analysis," *IEEE Access*, vol. 7, pp. 2520–2528, 2018.
[25] D. M. Pozar, *Microwave Engineering*, 2nd ed. Toronto, ON, Canada: Wiley, 1998.
[26] C. K. Lee and R. J. Langley, "Equivalent-circuit models for frequency-selective surfaces at oblique angles of incidence," *IEE Proc. H-Microw., Antennas Propag.*, vol. 132, no. 6, pp. 395–399, Oct. 1985.
[27] Q. Chen, D. Sang, M. Guo, and Y. Fu, "Frequency-selective rasorber with interabsorption band transparent window and interdigital resonator," *IEEE Trans. Antennas Propag.*, vol. 66, no. 8, pp. 4105–4114, Aug. 2018.
[28] M. Qu, S. Sun, L. Deng, and S. Li, "Design of a frequency-selective rasorber based on notch structure," *IEEE Access*, vol. 7, pp. 3704–3711, 2019.
[29] Q. Guo, Z. Li, J. Su, Y. L. Yang, and J. Song, "Dual-polarization absorptive/transmissive frequency selective surface based on tripole elements," *IEEE Antennas Wireless Propag. Lett.*, vol. 18, no. 5, pp. 961–965, May 2019.

XIMENG ZHANG was born in 1995. He received the B.S. degree in electronic science and technology from the University of Electronic Science and Technology of China, Chengdu, China, in 2017. He is currently pursuing the M.S. degree with the State Key Laboratory of Complex Electromagnetic Environmental Effects on Electronics and Information System, National University of Defense Technology, Changsha, China.

His current research interests include graphene, reconfigurable antenna, absorber, and frequency selective rasorber.

WEIWEI WU was born in 1981. She received the M.S. and Ph.D. degrees in electronic science and technology from the National University of Defense Technology, Changsha, China, in 2008 and 2011, respectively, where she is currently an Associate Professor with the State Key Laboratory of Complex Electromagnetic Environmental Effects on Electronics and Information Systems.

Her research interests include antennas design and wave propagation

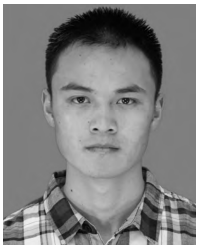

YUHONG MA was born in 1996. He received the B.S. degree in electronic science and technology from the National University of Defense Technology, in 2017, where he is currently pursuing the M.S. degree with the State Key Laboratory of Complex Electromagnetic Environmental Effects on Electronics and Information System.

His current research interests include RF/microwave circuits, ultra-wide-band technology, and microstrip antennas and filters.

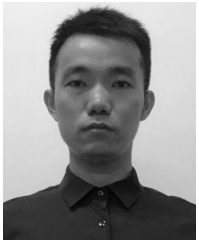

CHANG WANG was born in 1991. He received the B.S. degree in electronic engineering from the National University of Defense Technology, Changsha, China, in 2013, where he is currently pursuing the M.S. degree with the State Key Laboratory of Complex Electromagnetic Environmental Effects on Electronics and Information System.

His current research interests involve RF/microwave circuits and filters.

CHENXIN LI was born in 1995. She received the B.S. degree in electronic science and technology from Jilin University, Changchun, China, in 2017. She is currently pursuing the M.S. degree with the State Key Laboratory of Complex Electromagnetic Environmental Effects on Electronics and Information System, National University of Defense Technology, Changsha, China.

Her current research interests include phased array antenna and reconfigurable antenna.

NAICHANG YUAN was born in 1965. He received the M.S. and Ph.D. degrees in electronic science and technology from the University of Electronic Science and Technology of China, Chengdu, China, in 1991 and 1994, respectively. He is currently a Professor with the State Key Laboratory of Complex Electromagnetic Environmental Effects on Electronics and Information System, National University of Defense Technology, Changsha, China.

His research interests include microwave circuits design, wireless communication, and wave propagation.